AGU
ADVANCING EARTH AND SPACE SCIENCES

JGR Biogeosciences

RESEARCH ARTICLE

Key Points:
- Average NDVI values are used to derive distribution of salinity and organic mass accumulation rates in Terrebonne Bay, Louisiana
- NDVI reflects different plant types in the wetlands of Terrebonne Bay
- On average 0.065 g cm^{-2} yr^{-1} of organic mass are accumulated on a yearly basis in Terrebonne Bay

Supporting Information:

Supporting Information may be found in the online version of this article.

Correspondence to:

L. Cortese,
lucacort@bu.edu

Author Contributions:

Conceptualization: L. Cortese, S. Fagherazzi
Data curation: L. Cortese
Formal analysis: L. Cortese
Funding acquisition: L. Cortese, S. Fagherazzi
Investigation: L. Cortese, D. J. Jensen, M. Simard, S. Fagherazzi
Methodology: L. Cortese, S. Fagherazzi
Project Administration: S. Fagherazzi
Resources: L. Cortese
Software: L. Cortese
Supervision: L. Cortese
Visualization: L. Cortese, S. Fagherazzi
Writing – original draft: L. Cortese
Writing – review & editing: D. J. Jensen, M. Simard, S. Fagherazzi

Using Normalize Difference Vegetation Index to Infer Wetlands Salinity and Organic Contribution to Vertical Accretion Rates

L. Cortese[1] ◌, **D. J. Jensen[2]** ◌, **M. Simard[2]** ◌, **and S. Fagherazzi[1]** ◌

[1]Department of Earth and Environment, Boston University, Boston, MA, USA, [2]Jet Propulsion Laboratory, California Institute of Technology, Pasadena, CA, USA

Abstract Vegetation is a key component controlling soil accretion in coastal wetlands through production of belowground organic matter and enhanced deposition of mineral sediments. Vegetation structure is a proxy for wetland health and degradation that can be monitored at large scales with remote sensing. Among different multispectral indices, the Normalized Difference Vegetation Index (NDVI) is generally used for this purpose. Using Google Earth Engine (GEE), NDVI time-series are extracted around 45 monitoring stations of the Coastwide Reference Monitoring System (CRMS) located in Terrebonne Bay, Louisiana, USA. NDVI tends to increase from saline to freshwater wetlands. Using these NDVI observations and in situ measurements of salinity, soil accretion rates, and geomorphic metrics (i.e., elevation, distance from the bay or from the nearest channel bank), empirical models were developed to derive maps of organic mass accumulation rates and salinity. The analysis shows that NDVI can be used to reproduce the salinity gradient in Terrebonne Bay, as the index captures differences in vegetation cover, which depend on salinity. A negative relationship between NDVI and organic accumulation mass rates is also found, indicating that saline marshes tend to accumulate more organic material compared to fresh wetlands.

Plain Language Summary Coastal wetlands need to increase their elevation to counterbalance relative sea level rise. This process is achieved through deposition of mineral sediment and organic matter produced by local vegetation. The latter contribution becomes fundamental in areas lacking mineral supply. In this study, we show that it is possible to leverage on the Normalized Difference Vegetation Index (NDVI), a very common remote sensing indicator, to derive the contribution of vegetation to soil accumulation. Moreover, the same index can be used to derive the distribution of salinity. These results can be achieved because NDVI is related to the general plant type, which changes when we move from saline to freshwater wetlands.

1. Introduction

As sea level rises (SLR) and subsidence rates accelerate, coastal wetlands survival is determined by their ability to increase their surface elevation (Morris et al., 2002). In this accretionary process, wetlands heavily rely on vegetation to enhance deposition of suspended mineral sediment transported by tidal currents and storms, and on the accumulation of organic matter derived from vegetation (Booth et al., 2000; Christiansen et al., 2000; Nyman et al., 2006). However, in the last decades, the availability of mineral sediment from rivers has dropped, increasing the vulnerability of wetlands and deltas (Syvitski et al., 2009; Weston, 2014). In the particular case of the Louisiana's Mississippi River Delta Floodplain (MRDF), high rates of SLR (Sweet et al., 2022), enhanced subsidence due to human activities (Törnqvist et al., 2008), and a heavily reduced mineral sediment supply due to extensive damming (Blum & Roberts, 2009) have resulted in a loss of around 5,000 km^2 of wetland area in the last century (Couvillion et al., 2017). Therefore, it is imperative to characterize the spatial variability of the contribution of vegetation to soil accretion (i.e., organic accumulation rates) and environmental stressors that compromises plants productivity.

The classification of coastal wetlands in Louisiana is based on plant species and salinity, and vegetation cover is generally divided into saline, brackish, intermediate, and fresh (Nyman et al., 1993). With the only exception of the active deltas in the Atchafalaya Basin and the Mississippi birdfoot, brackish and freshwater wetlands located inland have suffered high losses with a consequent expansion of salt marshes (Chabreck & Linscombe, 1982; Valentine et al., 2021).

In coastal Louisiana, organic accumulation by vegetation is an important contribution to soil accretion (Nyman et al., 2006), even in areas located in the active deltas where there is constant supply of mineral sediment. Therefore, external stresses can be detrimental not solely on plant bioproductivity but also to the volume of organic mass deposited in the soil. Salinity is among the most impactful external stressors that drives ecological zonation of wetlands (Levine et al., 1998). Indeed, salinity has been found to be negatively correlated to aboveground biomass growth, and to impact productivity of salt marsh plants (Smart & Barko, 1980). Furthermore, salinity is the main driver of species abundance in saline deltas, compared to fresher areas, where species competition becomes a more important factor (Greiner La Peyre et al., 2001). Thus, high rates of SLR can be more detrimental to brackish and fresh wetlands as the enhanced flooding and saltwater intrusion can reduce soil organic carbon storage and aboveground biomass (Ewing, 1986; Ibñez et al., 2002; Janousek et al., 2020; Wilson et al., 2018). Consequently, being able to spatially characterize salinity, vegetation and organic accretion rates is crucial to predict the fate of Louisiana's coastal wetlands.

In situ measurements that provide high quality information can be used to directly derive spatial distributions of key variables. For instance, accretion rates can be measured in soil cores, sediment traps, soil horizon markers, pollen grains, and with radiometric dating based on ^{137}Ce and ^{210}Pb (Clark & Patterson, 1984; Donnelly & Bertness, 2001; Turner et al., 2000). In addition, from those measurements the organic and inorganic components can be separated (Morris et al., 2002; Neubauer, 2008; Sanks et al., 2020) and the data interpolated to infer spatial variability (Sanks et al., 2020). However, this approach is constrained by the limited accessibility of some locations and sparse spatial sampling. Different remote sensing sensors with very high spatial and temporal resolutions can be leveraged to fill this gap (Gallant, 2015). Multi-decade catalogues of images (e.g., Landsat program) are now available on cloud platforms (e.g., Google Earth Engine) to detect temporal trends.

Remote sensing imagery are valuable to spatially characterize wetlands. They allow to quantify wetland extent (Dong et al., 2014; Jia et al., 2014), map flooded areas (Li et al., 2015; Wang et al., 2002), and estimate wetlands carbon stocks (Crichton et al., 2015). Among the different indices that can be derived from multispectral sensors, the Normalized Difference Vegetation Index (NDVI) is often used to estimate the density of green vegetation in terrestrial ecosystems (Weier & Herring, 2000). NDVI is computed as the difference between the spectral reflectance in the red and the near-infrared regions divided by the sum. This index has been widely used to monitor wetlands (Guo et al., 2017). For instance, NDVI was successfully adopted to infer the Leaf Area Index of mangroves (Green et al., 1997; Kovacs et al., 2004), to monitor drought effects in Louisiana marshes (Mo et al., 2017) and to map marshes extent and change over time (Lopes et al., 2020). NDVI was also used to infer aboveground biomass in various wetland studies. For example, Tan et al. (2003) used Landsat-7 ETM + over the Poyang wetlands in China, observing that a change of 0.1 in NDVI produces a change of 500 g/m^2 of aboveground biomass. Lumbierres et al. (2017) modelled biomass production in the Doñana marsh (Spain) with MODIS derived NDVI. Doughty and Cavanaugh (2019) used NDVI derived from multispectral UAV imagery and estimated an average biomass peak of 1,200 g/m^2 at the Carpinteria Salt Marsh Reserve (California, USA).

However, an analysis of the relationship between remotely sensed measurements and organic deposition from vegetation has never been proposed. Recently, Jensen et al. (2022) derived accretion rates along coastal Louisiana using NDVI and estimated suspended sediment concentration from Landsat time-series as proxies for mineral and organic inputs respectively. Yet, no explicit relationship between NDVI and organic accretion was tested. Given the intrinsic relationship between NDVI and vegetation, it is hypothesized that NDVI correlates with the organic component of soil accretion and salinity. Such a relation would provide a tool to determine spatial patterns of two important parameters that control vulnerability and productivity of wetlands. Furthermore, the obtained maps could also be used to infer local carbon sequestration rates (Chmura et al., 2003) and support study on the impact of salinity on fishery and local fauna (Gunter, 1956; Reed et al., 2007).

2. Data and Methods

2.1. Location

The Terrebonne hydrological basin is located within the MRDF (Figure 1).

Due to the absence of major rivers and microtidal conditions, resuspension of bottom sediments during storm surges represents the main mechanism of mineral sediment distribution. Salinity follows a gradient from the saltier wetlands facing the Gulf of Mexico to the freshwater wetlands inland (Twilley et al., 2019). Four different
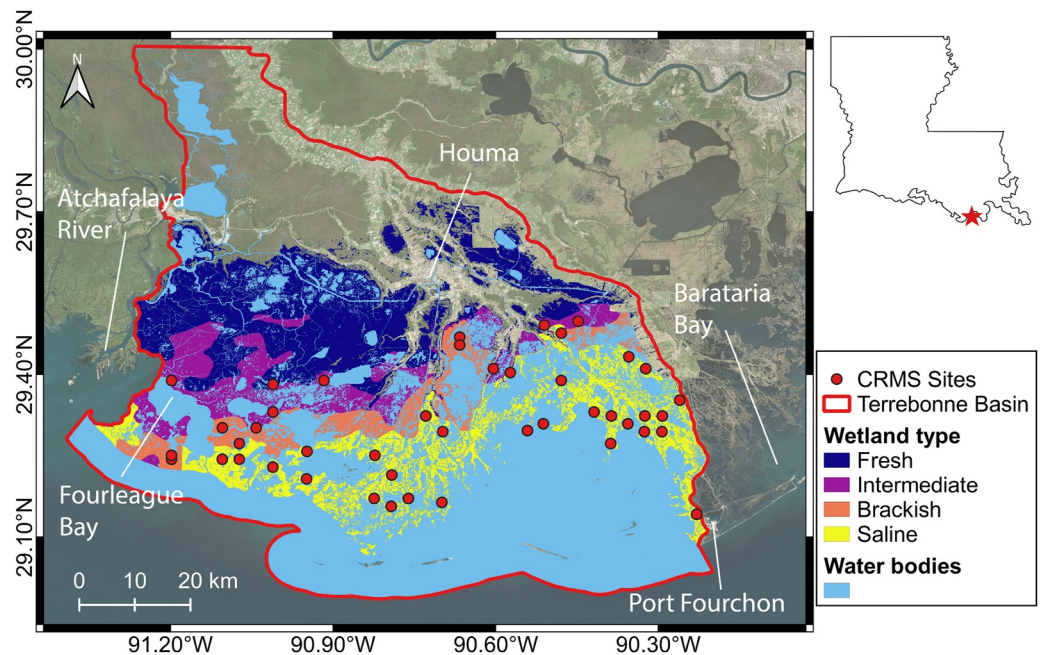
Figure 1. Terrebonne Bay and Terrebonne hydrological basin. Layers of the different wetland types are indicated. The CMRS sites are overlapped as red circles. On the upper-right corner, the red star locates Terrebonne Bay along the Louisiana Gulf coast.

types of wetlands can be classified based on salinity: saline, brackish, intermediate, and fresh (Sasser et al., 2014). Saline wetlands tend to be dominated by *Spartina alterniflora*, while *Spartina patens* is more common in brackish regions. Freshwater marsh vegetation is heterogeneous with a wider array of species (e.g., *Schoenoplectus americanus*, *Phragmites australis*).

2.2. Coastwide Reference Monitoring System Data

The Coastwide Reference Monitoring System (CRMS) is a project funded by the CWPPRA (Coastal Wetlands Planning, Protection, and Restoration Act) and encompasses around 390 monitoring sites distributed along the Louisiana coast. All available sites with a record of measured accretion were selected. In total, 45 monitoring sites located within the Terrebonne basin (see Table S1 in Supporting Information S1) were considered. At each site, collection of vertical accretion has started between 2006 and 2009 using feldspar marker horizons every 6/12 months. In addition to vertical accretion, for each station salinity timeseries, soil bulk density, elevation, and percentage of organic matter were retrieved. Finally, a wetland type was assigned to each site in 2021 (Nyman et al., 2022). Four vegetation classes were selected for this study: saline, brackish, intermediate, and fresh wetlands. Typically, brackish and intermediate wetlands could be merged, however this distinction was preserved herein. Nyman et al. (1993) observed that the intermediate class is separated from both fresh and brackish wetlands in terms of soil organic and inorganic composition. Overall, 25 sites were selected in saline wetlands, 12 in brackish wetlands, 6 in intermediate wetlands, and 2 in fresh wetlands.

2.3. Separation of the Mineral and Organic Contributions Mass Accumulation Rates

In each CRMS site there are multiple plots where accretion is regularly measured. The oldest plots are about 15 years old. One of the main challenges when comparing accretion rates measurements is the Sadler effect (Sadler, 1981). Accretion rates tend to decrease as the timescale increases because of soil compaction and general evolution of the system. Hence, it is important selecting accretion rates that cover a similar timespan. In order to have a reasonable number of samples, all available plots with at least 8 years of records were selected at each site (refer to Table S1 in Supporting Information S1). On average, the selected plots were 10 years old, with a 75th percentile of 12 years, indicating minimal influence of the Sadler effect. For each site, the accretion rates were

extracted from each plot and averaged. Soil bulk density (BD) and average percentage of organic matter (OM) was measured at 4 cm increments from 0 to 24 cm depth in two dates: on the establishment date of the oldest plot and in 2018. Given the average age of the plots and a mean total accretion rate of 1–1.5 cm/yr, only the first three layers (from 0 to 12 cm depth) were considered. To have a representative value for the entire period, the averaged values of BD and OM on the two collection dates were taken.

In order to separate the mineral and organic contributions to vertical accretion rates (VA), the procedure of Neubauer ([2008](#)) was followed. First, the organic bulk density (BD_O) was calculated as product between BD and OM, so that the mineral bulk density (BD_I) was computed as product between BD and (1-OM). Consequently, the organic and inorganic mass accumulation rates (OMAR and IMAR) were computed by multiplying the vertical accretion rates with BD_O and BD_I respectively (see Equations [1](#) and [2](#)).

$$OMAR = BD \cdot OM \cdot VA = BD_O \cdot VA \qquad (1)$$

$$IMAR = BD \cdot (1 - OM) \cdot VA = BD_I \cdot VA \qquad (2)$$

2.4. Spatial Data

For each site, distance from the channel, distance from the bay measured along the channel network, and direct distance from the bay were considered. For the three parameters, the values reported in Cortese and Fagherazzi ([2022](#)) were adopted. The term "channels" refers to the closest water body to a site, thus it can be either a channel, a lake, a small bay, or Terrebonne Bay itself (light blue areas in Figure [1](#)). The term "bay" refers to the coastline of Terrebonne Bay without the barrier island system of Isles Dernieres and Timbalier Island. Distance from the channel is the Euclidean distance computed between the vertical accretion sampling point and the nearest channel bank. Direct distance from the bay is defined as the shortest Euclidean distance to the coastline. Bathymetric data from NOAA Office for Coastal Management Coastal Inundation Digital Elevation Model were also retrieved (Love et al., [2010](#)). The DEM has a spatial resolution of 3 m, which was resampled to 30 m to match the Landsat data resolution (elevation map in reported in Figure S2 in Supporting Information [S1](#)). Since the presence of levees can highly influence sediment supply, GIS layers of leveed areas were retrieved for the Terrebonne Parish using the US Army Corps of Engineers National Levee Database (https://levees.sec.usace.army.mil/), and masked out from the computation. Spatial data of fractional floating vegetation (FAV) and fractional submerged vegetation (SAV) were retrieved from Couvillion ([2021a](#), [2021b](#)). These vegetation covers are mostly found in the north-western portion of the considered domain. Pixels with FAV and SAV cover over 20% were classified as water and masked out to limit uncertainty between wetlands and open water.

2.5. NDVI and Salinity Data

NDVI data from 2006 to 2021 were retrieved using GEE's Landsat catalog for the entire Terrebonne basin during the growing season (March–October, Myneni et al., [1997](#); Snedden et al., [2015](#)). All selected NDVI values are clouds, clouds shadows and snow masked. From all data, the average was computed to obtain a single NDVI value for each pixel. To isolate the NDVI values corresponding to the CRMS sites, the GIS shapefile layer was overlapped with the location of all sites to identify the correspondent pixel of the NDVI map.

Salinity timeseries started between 2006 and 2009 depending on the site and ended in 2021. To be consistent with NDVI, only salinity data during the growing season were considered and averaged to obtain one salinity value for each site. A two-cluster k-means classifier was applied to the NDVI map to derive a land-water mask in order to separate channels, lakes and bays from the marshland.

2.6. NDVI Analysis and Models to Retrieve Organic Mass Accumulation Rates and Salinity

First, NDVI values were separated based on the wetland type, and the presence of statistical differences between each group was tested. To do so, a one-way analysis of variance (ANOVA) followed by a Tukey's honestly significant difference (HSD) post-hoc test was used (Abdi & Williams, [2010](#)).

Then, to observe whether a relationship between NDVI and geomorphic metrics exists, the average NDVI at each CRMS site was compared with distance from the channel, distance from the bay, direct distance from the bay, and site elevation using bivariate linear regressions.

To develop models of organic mass accumulation rates (OMAR) and salinity, the datasets were randomly separated into a training and testing sets. The training dataset took 60% of the data, while the remaining 40% was allocated to testing. Models were inferred with multivariate linear regressions using a backward stepwise selection. Thus, starting with the full models, which included NDVI and all geomorphological variables as independent variables, the least significant variable (highest p-value) was removed at each step, until all variables left had a p-value smaller than the 0.05 threshold. To test whether it was possible to derive a model of NDVI from all geomorphological variables, the backward stepwise regression was applied to find the best multivariate model to predict NDVI given the distance from the channel and from the bay, direct distance from the bay, and marsh elevation.

To evaluate models performance, besides the R^2 for bivariate correlation and the adjusted R^2 for the multivariate correlations, the Root Mean Squared Error (RMSE) was adopted, defined as the squared root of the average of the squared differences between the observed and modeled values. RMSE was chosen because has the same unit of the modeled variables. An analysis on the residuals was performed to verify the correctness of the linearity hypothesis. On the residuals, we tested normality, homoscedasticity, presence of outliers, and independence.

The models were applied on the entire domain to obtain maps of OMAR and salinity. A NDVI map was also derived from geomorphic parameters. The models were spatially applied using the NDVI raster, the DEM, and the distance form channel and bay.

3. Results

3.1. Organic and Inorganic Contributions to Soil Vertical Accretion Rates

Results show that inorganic mass accumulation rates are greater than organic ones, however the organic accretion rates have higher leverage in terms of volume given the lower density (Figures 2a and 2b). A significant positive linear correlation was found between total accretion rates and both mineral and organic accumulations. In particular, the latter case gave a R^2 of 0.92.

A one-way ANOVA revealed that there is no significant difference in the mean OMAR values between the different wetland types (Figure 2c), while the same test showed that inorganic accumulation rates in saline wetlands are statistically different from brackish and intermediate (Figure 2d, Tables S2 and S3 in Supporting Information S1).

3.2. NDVI and Wetland Type

NDVI values display different ranges depending on the wetland type (Figure 3). Overall, the distributions indicate increasing values moving from saline wetlands toward the fresh ones. Saline wetlands display the wider range of NDVI (0.1–0.6), with an interquartile range (IQR) between 0.3 and 0.47. Brackish wetlands have a narrower range, with values in the IQR of 0.42–0.54. Intermediate wetlands IQR varies between 0.53 and 0.64, whereas NDVI values of fresh wetlands have a higher IQR from 0.65 to 0.79. Furthermore, a one-way ANOVA and the Tukey post-hoc test confirmed that there is a statistically significant difference between the means of each group (see Tables S4 and S5 in Supporting Information S1).

3.3. NDVI and Geomorphological Parameters

A positive linear correlation was found between NDVI and distance from the nearby channel (Figure 4a), indicating the tendency for the NDVI to increase when moving away from the banks. Despite the satisfactory p-value, the $R^2 = 0.273$ indicates that this variable cannot capture much of the variability of NDVI. Results improved when both distance from the bay along the channels and direct distance from the bay (Figures 4b and 4c) are considered, for which positive logarithmic regressions have low p-value and R^2 of 0.473 and 0.462 respectively, indicating a higher explanatory ability. Elevation is the only variable found not statistically correlated to NDVI (Figure 4d).

3.4. Multivariate Regressions for Salinity, Organic Mass Accumulation Rates, and NDVI

All models for salinity, OMAR, and NDVI obtained with the backward stepwise regressions are reported in Table 2. For a detailed report of all the steps carried out for each model and p-values refer to Tables S6, S7, and
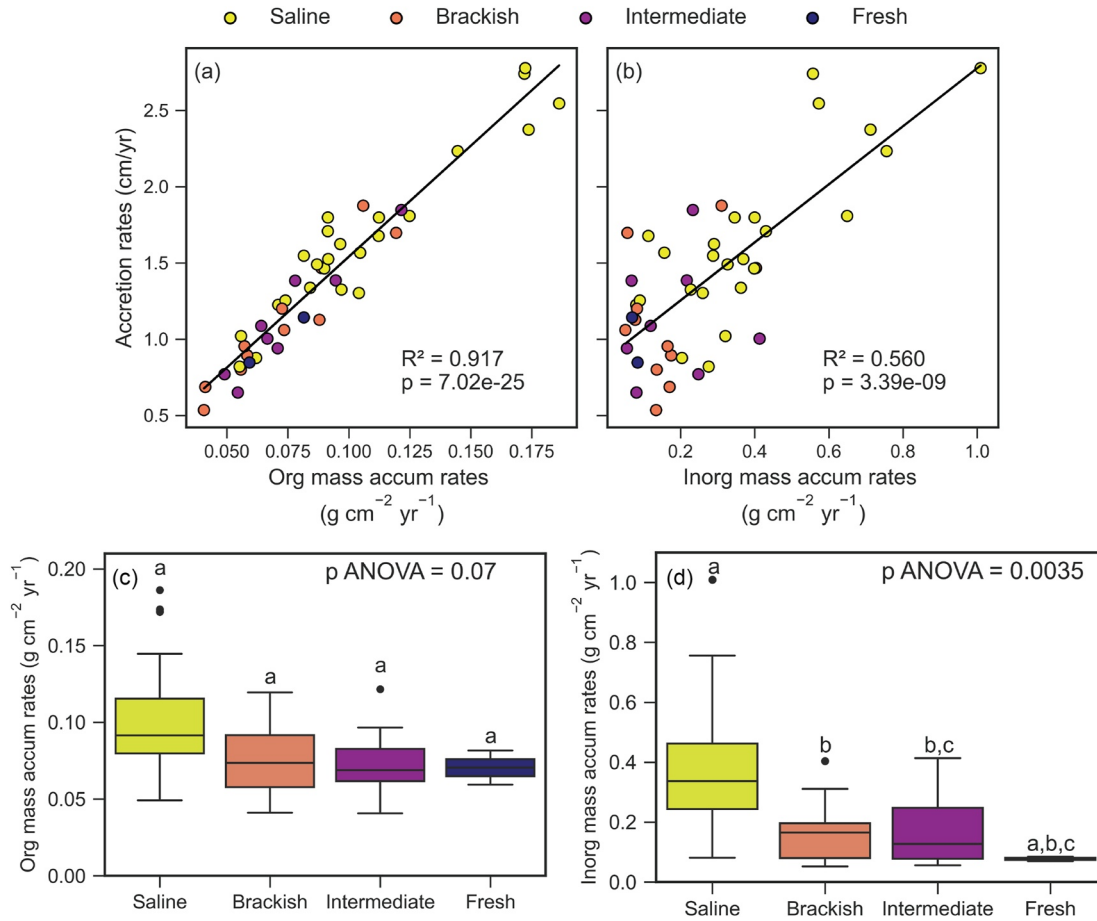
Figure 2. Correlation between total accretion rates and (a) organic accretion rates and organic mass accumulations rates, (b) inorganic accretion rates and inorganic mass accumulation rates. (c) Boxplots showing the distribution of organic mass accumulation rates in each vegetation zone. (d) Boxplots showing the distribution of inorganic mass accumulation rates in each vegetation zone. Different letter on top of the boxplot indicates that the distribution is statistically different ($p < 0.05$, Tukey's HSD). The main body of the boxes shows the 25th, 50th (median), and 75th percentiles. The whiskers extend to the extreme values that are not considered outliers.

S8 in Supporting Information S1. Tests on residuals confirmed the goodness of the hypothesis of linearity (Tables S11, S12, S13 in Supporting Information S1).
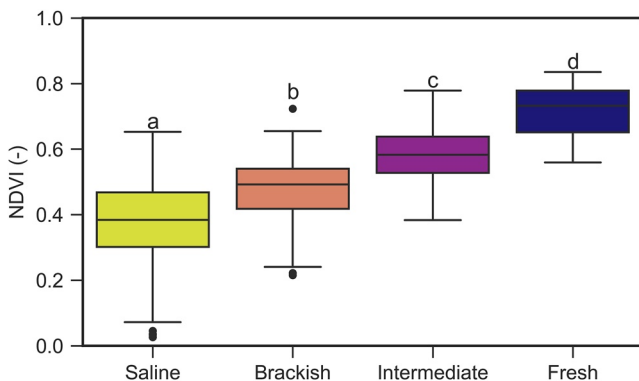
Figure 3. Boxplots showing distribution of all CRMS NDVI values for each wetland type. The main body of the box shows the 25th, 50th (median), and 75th percentiles. The whiskers extend to the extreme values that are not considered outliers. Different letter on top of the boxplot indicates that the distribution is statistically different ($p < 0.05$, Tukey's HSD).

After all steps, the statistically significant OMAR model considered only NDVI as independent variable, with an R^2 and RMSE of 0.485 and 0.028 g cm^{-2} yr^{-1} for the training data, and 0.325 and 0.033 g cm^{-2} yr^{-1} for the testing data (Figures 5a and 5b). The model showed a negative linear relationship with NDVI, indicating that areas with lower NDVI in Terrebonne Bay, which tends to be closer to the coast, have higher organic mass accumulation compared to areas located inland, where NDVI tends to increase (Figure 6). By applying the model to the entire domain, it was estimated an average 0.065 ± 0.035 g cm^{-2} yr^{-1} of organic mass accumulated on a yearly basis.

The most statistically significant model to predict salinity included NDVI and wetland elevation (Figures 5c and 5d and Table 2). Model training provided an R^2 and RMSE of 0.6 and 3.74 ppt, respectively, whereas the testing provided an R^2 and RMSE of 0.531 and 3.96 ppt, respectively. The model showed salinity being negatively correlated with NDVI and wetland elevation, indicating that areas closer to the coast (which present a lower NDVI) have higher salinity compared to fresher ones, which have higher NDVI and
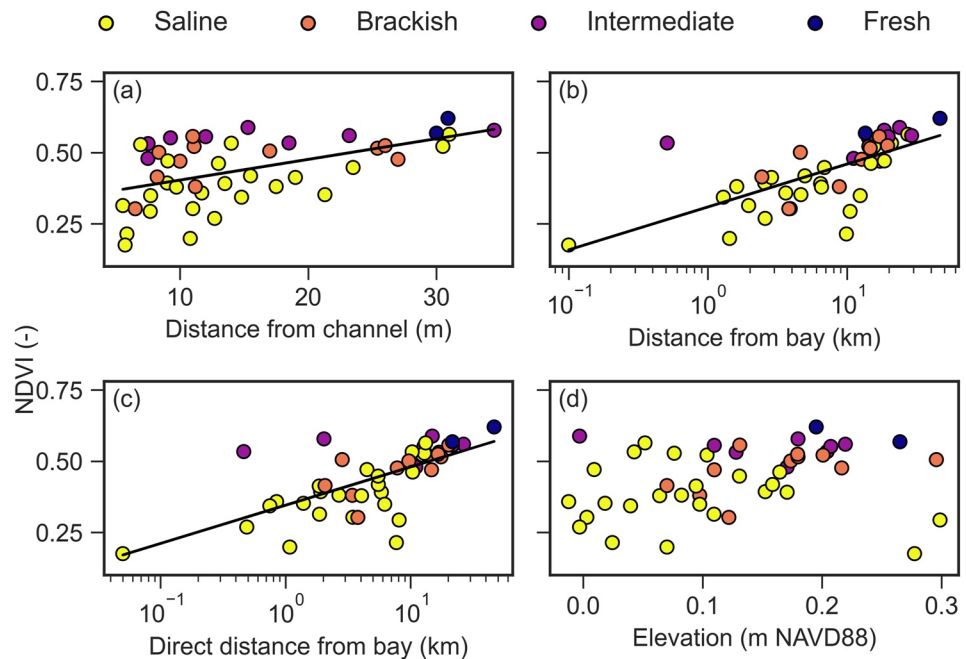
Figure 4. Regression plots between NDVI and geomorphological variables. (a) Distance from the channel, (b) Distance from the bay, (c) Direct distance from the bay, and (d) wetland elevation. When the regression is not statistically significant, the regression line is omitted. R^2 and *p*-values are reported in Table 1. Note that subplots (b) and (c) have logarithmic scale for the *x*-axis.

are found further inland. It was also verified that the model is able to identify the different wetland types. To do so, each pixel of the salinity map was assigned to the correspondent vegetation category using the vegetation map (Figure 8). Results of ANOVA and Tukey's HSD post-hoc test (see Tables S9 and S10 in Supporting Information S1) confirmed that means of each group are statistically different from one another.

The third model predicts the distribution of NDVI using distance from the bay and distance from the channels (Figure 9a). In particular, NDVI is predicted to increase with both variables (Figures 5e and 5f, Table 2). The training provided an R^2 and RMSE of 0.61 and 0.07, respectively, whereas the testing provided an R^2 and RMSE of 0.52 and 0.08, respectively.

While the distribution showed a coherent gradient increasing from the coast to the inland, there are some parts of the domain where the model tends to overestimate or underestimate the measured NDVI (Figure 9b and Figure S1 in Supporting Information S1). In particular, the model overestimates the NDVI in some areas located in the intermediate and fresh wetlands, while the NDVI in the central saline wetland and south-western area portion adjacent to Fourleague Bay is underestimated. NDVI is underestimated in the southern-central tip of the bay and in the Port Fourchon area. Here NDVI is likely higher due to the presence of black mangroves (Osland et al., 2020), that cannot be captured by the model.

Table 1
R^2 and p-Values of Regressions Between NDVI and Geomorphological Variables

Independent variable	R^2	*p*-value	Slope	Intercept
Distance from channel bank (m)	0.273	2.23E−04	0.007	0.331
Distance from the bay (km)*	0.473	1.81E−07	0.065	0.309
Direct distance from the bay (km)*	0.463	2.75E−07	0.058	0.345
Elevation (m NAVD88)	0.063	0.0974	0.343	0.397

Note. Since multiple comparisons are performed at the same time, the Bonferroni adjustment is used to set a more conservative *p*-value. Given the four variables we set the threshold at 0.05/4 = 0.0125. Values with the * indicates logarithmic regressions.

Table 2
Models of Organic Mass Accumulation Rates, Salinity, and NDVI

Y	Model	RMSE training	RMSE testing	R^2 training	R^2 testing
OMAR (g cm^{-2} yr^{-1})	$0.195-0.241 \cdot NDVI$	0.028	0.033	0.485	0.325
Salinity (ppt)	$29.08-32.02 \cdot NDVI -24.10 \cdot elev$	3.739	3.960	0.600	0.531
NDVI (−)	$0.308 + 0.0003 d_c + 0.007 d_b$	0.071	0.084	0.606	0.525

Note. For each variable, the full model is reported with corresponding RMSE and R^2 for the training and testing datasets. d_c and d_b indicate distance from the channel and distance from the bay respectively. For the *p*-values refer to Tables S6, S7, and S8 in Supporting Information S1. The RMSE has the same unit of the dependent variable Y.

4. Discussion

4.1. NDVI and Physical Parameters

The third model in Table 2 shows that NDVI tends to increase with distance from the bay and from the nearest channel. The NDVI distribution calculated from the landscape geometry shows an increasing upward gradient going from an average of 0.3 in the saline wetlands to 0.75 in the fresh wetlands. This result is coherent with the NDVI values extracted from GEE and previous studies (e.g., Suir & Sasser, 2019). As previously pointed out and shown in Figure 9, there are some areas in the map where NDVI is overestimated with values around the 0.95–1. This result is likely due to the water mask adopted to compute the distance from the channels. In order to be consistent with the Landsat image, a 30 m water mask was adopted, which is not able to detect the narrow channel networks in those areas, causing an over estimation of the distance from the channels and subsequently of NDVI. In the Port Fourchon area and along the southern tip of the basin, the encroachment of mangroves has been observed in recent years (Osland et al., 2020). In Figure 9b, we detect NDVI values between 0.7 and 0.8 for mangroves, which are consistent with values measured in North America (Ruan et al., 2022). The model clearly underestimates these values, because it has no information regarding this type of vegetation (none of the CRMS locations used to parametrize the model is located in mangroves). The model underestimates NDVI in the south-western portion of the domain that is adjacent to Fourleague Bay. The underestimation could be a reflection of a different landscape, as this area has been found to be hydrologically influenced by the Atchafalaya River and to show a distribution of vegetation zones typical of an active deltaic coastal basin, compared to the inactive Terrebonne Bay (Twilley et al., 2016, 2019).

Figure 3 shows that NDVI can be used to identify the different vegetation zones, which suggests that NDVI is tightly related to the vegetation species and general plant communities that dominate each zone (Kearney et al., 2009; Sun et al., 2018; Zhang et al., 1997). Saline wetlands, which are located in proximity to the coast, are dominated by *S. alterniflora*, while in brackish wetlands *S. patens* is the primary species. In both cases, several brown stems (necromass) are present in the vegetation canopy. Moving into intermediate and fresh wetlands, species composition becomes more heterogeneous but generally large-leafed herbs dominated, such as *Sagittaria lancifolia*, *Hydrocotlye umbellata*, and *Zizaniopsis miliacea*. These morphological plant differences are controlled by the geomorphological parameters, especially the distance from the bay. *Spartina* spp. found near the coast have lower NDVI, compared to freshwater species located farther inland that appear greener during the growing season because of broad leaves. The positive correlation with distance from the channel indicates that NDVI increases in areas further away from the creek. This is an unexpected result and could be a reflection of the specific CRMS points considered rather than a general pattern, and the limitations given by the Landsat resolution. Measured distances range from a few meters to 35 m (see Figure 4a), with most sites located 10–15 m from the channels, while each Landsat pixel is 30 by 30 m. Thus, it is not possible to capture NDVI differences at such small scale. Furthermore, despite the statistically significant correlation (Table 1), the low R^2 indicates that distance from the channel captures a minimal portion of the NDVI variability.

As noted by DeLaune et al. (1979), the typical geomorphic configuration of Terrebonne Bay is high natural levees at channels banks and low inland areas. The levees tend to have a higher mineral sediment fraction, which leads to higher bulk densities able to sustain denser, taller, and more vigorous *S. alterniflora*. Inland plants are typically shorter and sparser. For this reason, it is reasonable to expect a negative correlation between NDVI and distance from the channel due to the levees effect.
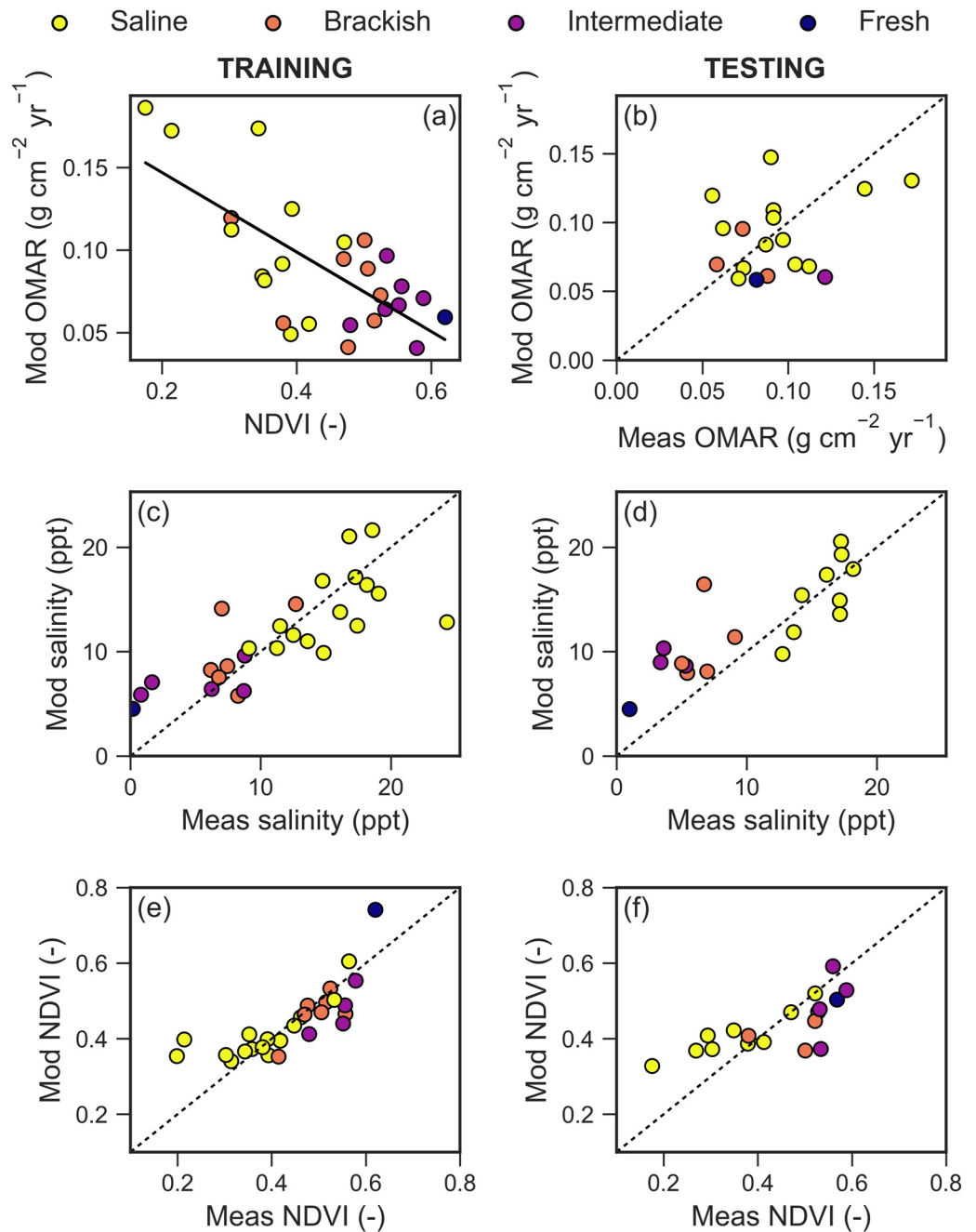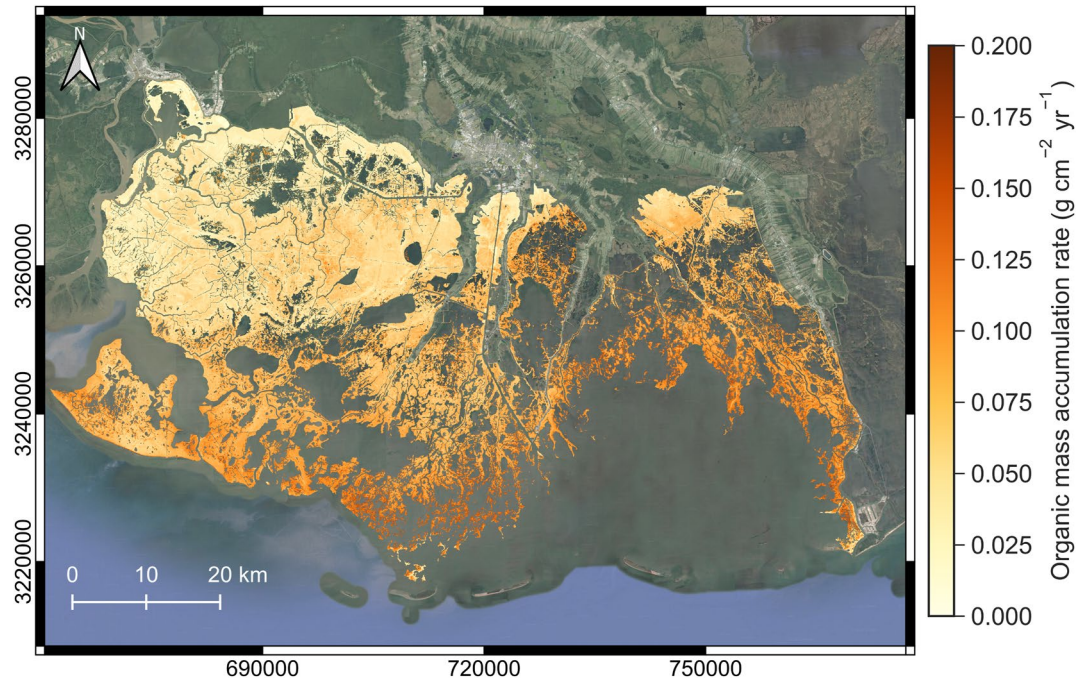
Figure 5. Models of organic mass accumulation rates (a),(b), salinity (c),(d), and NDVI (e),(f). The left column displays the training, while the right column the testing. Note that there is a one on one comparison in all testing subplots. Only subplots (a) shows the model, because (c) and (e) models cannot be displayed in a bidimensional space.
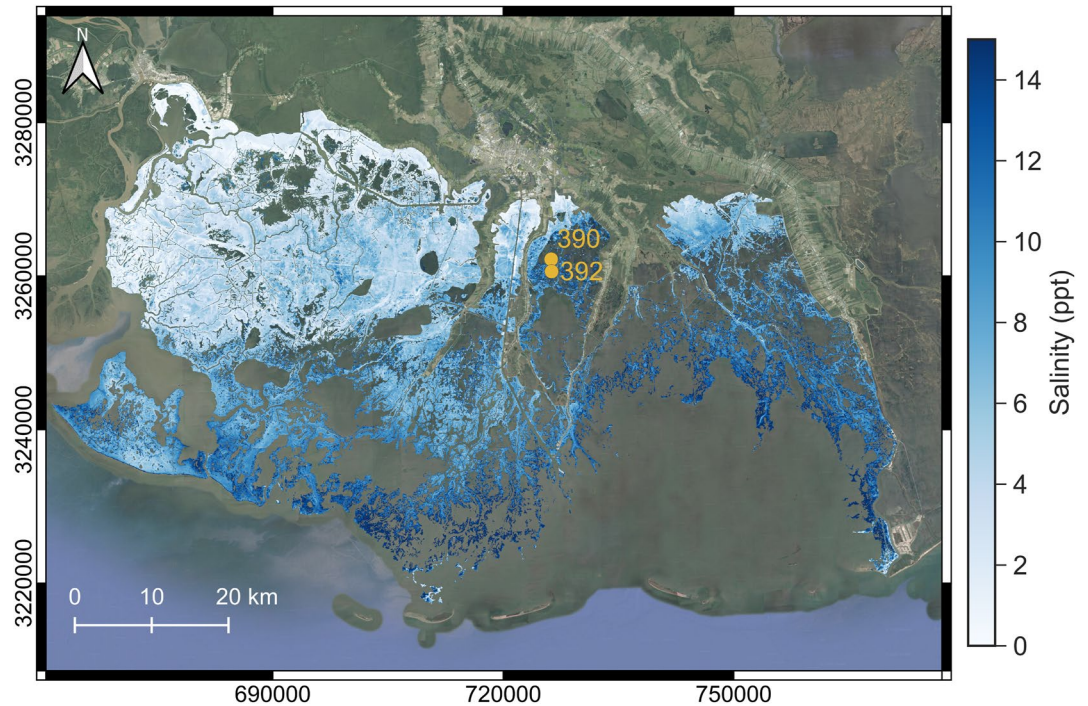
4.2. NDVI and Salinity

The relationship between NDVI and salinity found here is consistent with previous studies. NDVI tends to increase moving from saline marshes toward fresh wetlands, explaining the correlation between NDVI and salinity (Mo et al., 2015; Tilley et al., 2007). This is further confirmed by the analyses reported in Figures 4c and 4d and 7 and 8.

The salinity gradient showed in Figure 7 is a consequence of the low riverine input in the basin. Indeed, Terrebonne Bay vegetation cover is classified as 50% saline, 20% brackish/intermediate, 20% freshwater and 10% swamp (Twilley et al., 2019). The second multivariate model in Table 2 shows a negative relationship of salinity with NDVI and elevation.

Figure 6. Distribution of organic mass accumulation rates in Terrebonne wetlands computed with NDVI.

A decreasing trend of salinity with elevation is consistent with the fact that low elevation combined with SLR increases the likelihood of prolonged inundation and saline intrusion (Cahoon & Reed, 1995; Costa et al., 2023). Interestingly, marsh elevation does not homogeneously increase moving inland (Figure S3 in Supporting Information S1) and relatively high elevation areas near the coast promote brackish vegetation (Figure S4 in Supporting

Figure 7. Salinity distribution in Terrebonne Bay derived from NDVI and wetland elevation above/below NAVD88. The location of stations 390 and 392 is also indicated. The upper value of the colorbar is limited to 15 ppt to enhance contrast between different areas.
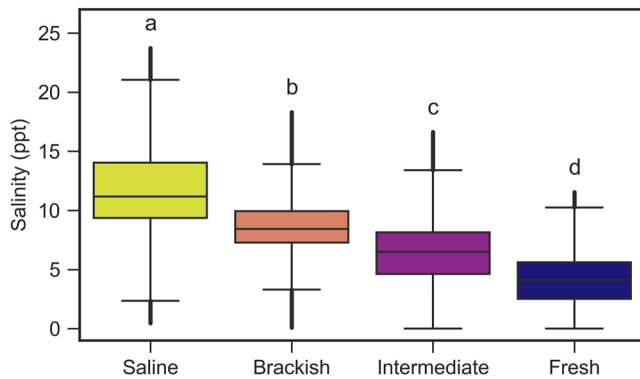
Figure 8. Salinity distribution in different wetland types obtained from the salinity model. The main body of the box shows the 25th, 50th (median), and 75th percentiles. The whiskers extend to the extreme values that are not considered outliers. Different letters on top of the boxplot indicates that the distribution is statistically different ($p < 0.05$, Tukey's HSD).

Information S1). The negative correlation between salinity and NDVI is tightly related to vegetation characteristics. As previously discussed, NDVI is an expression of vegetation communities and depends on the dominant species in a specific zone. Thus, NDVI can be used to recognize vegetation zonation (Figure 8), which is tightly related to plant salt tolerance (Greiner La Peyre et al., 2001). In Louisiana, *S. alterniflora* and *S. patens* dominate salt marshes due to their high tolerance to salt and flooding, whereas freshwater species are confined to inland wetlands because they cannot withstand these high abiotic stresses (Engels & Jensen, 2010).

Our results show high salinity values in some areas that might not reflect true conditions (Figure 7). The zone of Bayou Petit Gaillou and Lake Boudreaux south of Houma (where stations 390 and 392 are located) has the highest values of salinity of all the brackish wetlands. This portion of the basin has gone through a constant land loss process (Couvillion et al., 2017), which increased the open water area and consequently decreased vegetation cover and NDVI. Moreover, this area is hydrologically disconnected from the bay as a result of the construction of Highways 56 and 57. The high subsidence rates combined with reduced sediment supply has triggered the elevation drop (Yuill et al., 2009). The combination of decreasing NDVI and elevation affected the salinity calculation from the model, producing an overestimation compared to the measured values (7.02 and 6.73 ppt measured and 13.11 and 14.53 modeled in station 390 and 392, respectively). Moreover, in the north-western portion of the domain there are some unrealistic values within the freshwater wetlands. Despite masking floating and submerged vegetation from the analysis, it is possible that some areas with this vegetation cover were included, thus generating high salinity values. From Figure 7 it can also be observed that the eastern salt marshes are characterized by higher salinity compared to the western ones. One reason could be that, despite being both close to the bay, the eastern side is highly fragmented and consequently highly connected to the bay, allowing the propagation of saline water coming from the Gulf of Mexico. Moreover, the western side of Terrebonne could be affected by Fourleague Bay, the dynamics of which are regulated by fresh water discharged by the Atchafalaya River (Perez et al., 2000; Wang et al., 1995).

4.3. NDVI and Organic Mass Accumulation Rates

The separation of the organic and mineral contributions to accretion showed that total accretion is highly correlated with OMAR (Figure 2a). In coastal Louisiana, the linear correlation between the two variables was already presented in previous studies. Turner et al. (2000) and Neubauer (2008) proposed similar relationships for both salt and freshwater marshes respectively, while Kelsall et al. (2023) found a linear correlation between total vertical accretion and soil carbon stock. Despite the ANOVA analysis did not detect an overall difference between wetland types in terms of organic contribution (Figure 2c), boxplots display a tendency of higher OMAR in saline wetlands. This is also captured by the first model in Table 2, which linearly relates NDVI to OMAR. In particular, the model shows that OMAR tends to increase as NDVI decreases. Salt marshes have not only higher OMAR but also higher inorganic sediment load (Figures 2b and 2d). Since Terrebonne is an inactive basin of the MRDF, the sources of inorganic sediment are the Gulf of Mexico and the bottom of local channels and bays. The mineral sediment is then brought to the marsh surface through tidal inundation and storm surges. Thus, saline marshes show higher sediment loads compared to freshwater marshes because they are much closer to the mineral sediment sources.

An extensive body of research indicates that inorganic sediment availability influences the vegetation OMAR. Salt marshes are dominated by *S. alterniflora*, which requires higher soil bulk densities compared to *S. patens* and freshwater species (DeLaune et al., 1979). In particular, this species requires more mineral supply. Indeed, for the same rate of submergence, salt marshes need twice the amount of inorganic sediment as they are subjected to toxic sulfite generated in reduced conditions, while freshwater marshes can rely more on organic matter to balance SLR (Nyman et al., 1990). Salt marshes also need more organic accumulation to produce the same accretion (Nyman et al., 2006). At the same time, a higher sediment load favors bioproductivity and soil organic carbon accumulation because it reduces the concentration of phototoxins by improving soil aeration and provides nutrients to the plants sustainment (DeLaune & Pezeshki, 1994; Kelsall et al., 2023; Mendelssohn & Kuhn, 2003), therefore, despite representing a small contribution in volumetric terms, inorganic sediment remains an important factor for the overall survival of wetlands. Indeed, the lack of mineral load in brackish and fresh areas has
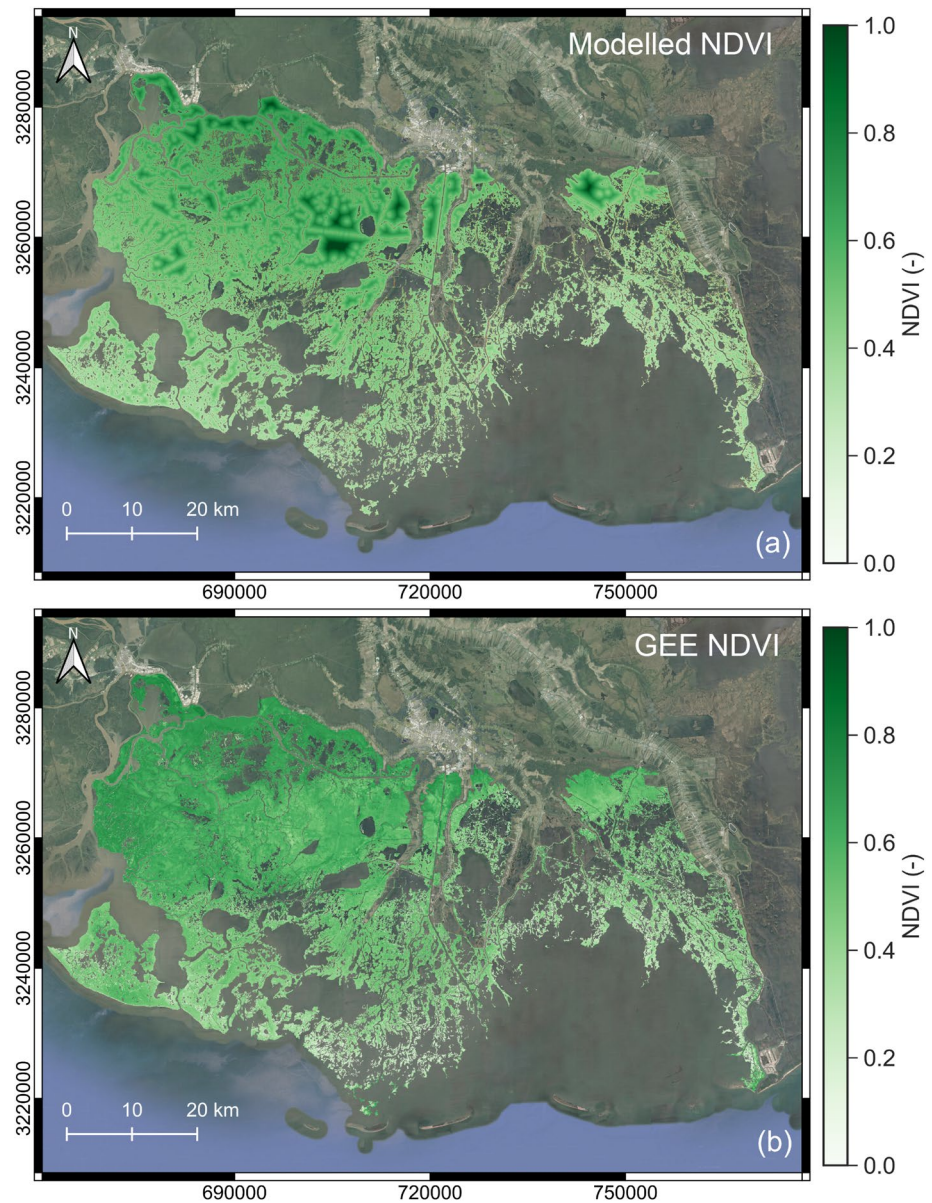
Figure 9. (a) Average NDVI distribution in Terrebonne Bay calculated from geomorphological variables. (b) Average NDVI between 2006 and 2021 during the growing season extracted with Google Earth Engine.

been linked to higher rates of wetland loss compared to saline wetlands. Fresh wetlands also have lower shear strength which makes them vulnerable to high shear stresses during major events and interior pond expansion (Howes et al., 2010; Valentine et al., 2021). An additional contribution to the higher OMAR in saline marshes is the enhancement of belowground production by the system of roots and rhizomes typical of *Spartina alterniflora* (Bertness, 1991; Howes et al., 1981). These species have a dense root network penetrating the soil up to a 30 cm depth (Chung, 2006; Darby & Turner, 2008). On the contrary, *S. patens* roots are depth-limited due to a lower tolerance to anoxic conditions (Bertness, 1991). The denser and deeper roots of *S. alterniflora* is also reflected in the larger amount of live biomass found at different depths compared to *S. patens* (Connor & Chmura, 2000). Belowground productivity of *S. patens* has been also found to be more sensitive to increase in hydroperiod and decrease more rapidly compared to *S. alterniflora* (Snedden et al., 2015).

In the nearby Atchafalaya basin, not only there is a net positive land gain (Couvillion et al., 2017; Jensen et al., 2022), but also healthy and stable freshwater wetlands due to mineral sediment supply from the rivers (DeLaune et al., 2003, 2016). On the contrary, the isolated brackish and freshwater marshes in Terrebonne do

not receive the critical mineral sediment supply that allows marshes to sustain plant growth and keep pace with rising waters (DeLaune et al., 1979, 2013). Here, the lack of mineral sediment inputs combined with subsidence rates and high salinity increases vegetation stress and reduces bioproductivity (Krauss et al., 2009), suggesting a possible decrease in organic contribution to accretion.

The linear model used to compute OMAR provided an average of 0.065 g cm^{-2} yr^{-1}. Previous studies used field measurements of accretion rates to compute organic accumulation, and can be used to evaluate the results of our study. For instance, Turner et al. (2000) collected measurements of accretion rates from ^{137}Cs in the Terrebonne and Barataria basins, and found a range between 0.02 and 0.1 g cm^{-2} yr^{-1} with an average OMAR of 0.049 g cm^{-2} yr^{-1}. In this case, it as to be considered that the accretion rates measurements consider a longer time period (from 1963/1964) compared to this analysis, thus organic decomposition and the Sadler effect (Sadler, 1981) could be non-neglectable factors. More recently, Sanks et al. (2020) spatially interpolated the CRMS vertical accretion data along the entire Louisiana coast using Bayesian kriging. They found an average OMAR of 0.092 g cm^{-2} yr^{-1} in Terrebonne, larger than our values. The discrepancy could be connected to the inherent limitations of the NDVI approach (which are discussed in Section 4.4). However, it has also to be noted that Sanks et al. (2020) performed the interpolation on a 1 km^2 grid. In our study, given the 30 m Landsat resolution, the pixel area is 0.0009 km^2. Therefore, we can capture more spatial variability in OMAR. At a lower resolution, features such as channels and ponds could not be recognized. Furthermore, the CRMS might not be statistically well distributed, thus affecting the overall average. This can cause a disproportional coverage of one vegetation type compared to others. One of the advantages of the remote sensing approach is that the vegetation variability across the landscape is better captured due to NDVI information at the small scale.

The method proposed herein shows that it is possible to leverage on remote sensing to infer the accumulation of organic matter along the Louisiana coast. Moreover, the method overcame the limitation of point measurements and retained the details of moderate resolution remote sensing images (tens of meters). This method allowed the separation of the contribution of the different areas of the wetland.

The great advantage of remote sensing (and especially of the Landsat program) is the availability of imagery globally for multiple years. Moreover, cloud computing platforms such as GEE, make the access to these data easier. The method needs extensive local data to establish a relationship between NDVI and OMAR. Therefore, this methodology could be applied in marshes outside coastal Louisiana where multiple measurements are available. The method could also provide a first order approximation of OMAR in areas where there is paucity of data but where vegetation communities, climate, and edaphic characteristics are similar.

4.4. Limitations of the Approach

It must be noted that the OMAR model does not yield a high R^2 (especially for testing). This indicates that NDVI only partially captures the OMAR variability and that other factors need to be accounted for. The use of a linear relationship can be a limitation, since ecological processes involved in accretion can be non-linear (Ryo & Rillig, 2017). Despite the CRMS offers an extensive dataset, the model was trained and tested on a dataset of 45 total locations. The use of a larger dataset might be helpful for improving the relationship. The elevation parameter was not included in the model because it resulted to be non-significant (high p-value). However, marsh elevation could play a role into organic accretion since it regulates the hydroperiod (i.e., the submergence period) that ultimately controls vegetation cover. As mentioned earlier, the model was trained and validated in only one Bay, therefore before deriving general conclusions for the entire MRDF further analysis should be considered. In particular, the method should be first applied on a basin affected by similar dynamics. An example could be the nearby Barataria Bay, which like Terrebonne, had the sediment supply from the Mississippi River cut off due to the construction of levees. The method should also be tested along the active deltaic regions, where the riverine sediment load provides large volumes of mineral sediment and allows vegetation establishment.

Future work could also investigate whether the relationship between NDVI and OMAR is dependent on vegetation type. Mo et al. (2018) showed that there are strong variations in Leaf Area Index (LAI) in fresh and saline marshes. Since LAI is highly correlated to NDVI, it is reasonable to assume a dependency of the NDVI-OMAR relationship on the vegetation type. In this case, such a separation was not possible due to the limited dataset, but a separation by wetland type could be explored by considering the entire MRDF.

Finally, it is worth mentioning that this analysis was limited to NDVI, therefore future work should also consider exploring the use of different spectral indices and their combinations. Indices such as the Enhanced Vegetation

Index (EVI; Huete et al., 1999) and Soil-Adjusted Vegetation Index (SAVI; Huete, 1988), might provide additional information able to improve model results, as they have been found to be effective in salt marsh classifications (Sun et al., 2020).

5. Conclusions

This study tested whether NDVI could be used as a proxy to estimate salinity gradients and the organic contribution to accretion in Terrebonne Bay, Louisiana USA. When the mineral and organic contributions to accretion were separated, a high correlation was found between total accretion rates and organic accretion rates, confirming the primary role of vegetation on vertical accretion. The analysis determined that marshes with high organic mass accumulation are also those with high inorganic mass accumulation rates. It was also determined that NDVI is strongly related to the geomorphology of the wetlands: NDVI increases with distance from the nearby channel and with the overall distance from Terrebonne Bay. A model that includes NDVI and elevation was able to separate different wetland types and provide the spatial distribution of salinity coherent with vegetation surveys. Finally, a negative linear relationship was found between organic mass accumulation rates and NDVI. From the model we obtained an average OMAR of 0.065 g cm^{-2} yr^{-1}. The spatial distribution of OMAR indicates that saline marshes in Louisiana tends to accumulate more organic mass compared to freshwater ones. This study shows that remote sensing data, and especially a common index as NDVI, can be used to spatially characterize important indicators of wetlands vulnerability. Most importantly, the analysis suggested that in coastal marshes NDVI is expression of belowground productivity because it captures plant types and vegetation zones.

Data Availability Statement

Data supporting the findings are publicly available. Soil accretion, soil bulk density, and soil organic content data used to separate the inorganic and organic contributions to accretion can be downloaded via the CRMS website (https://cims.coastal.louisiana.gov/monitoring-data/). From the same website were downloaded salinity data and location of the CRMS sites. The vegetation types map used to separate the marsh in saline, brackish, intermediate, and fresh can be found via the USGS website (https://www.sciencebase.gov/catalog/item/624d-dd6ad34e21f82766a252) (Nyman et al., 2022). Bathymetric data used to derive marsh elevation are available via the National Center for Environmental Information website (https://www.ncei.noaa.gov/access/metadata/landing-page/bin/iso?id=gov.noaa.ngdc.mgg.dem:1521) (Love et al., 2010). Spatial data of fractional floating vegetation (FAV) and fractional submerged vegetation (SAV) used to mask out areas that could be interpreted as wetlands were retrieved from the USGS website via (https://www.sciencebase.gov/catalog/item/606df312d34e-ae125e9c7647) (Couvillion, 2021a, 2021b). Geomorphological data of distance from the channel, and distance from the bay used to derive the models were taken from Cortese and Fagherazzi (2022). Spatial data of leveed areas, which were masked out from the calculations can be downloaded via the National Levee Database (https://levees.sec.usace.army.mil/). The Landsat data catalog is available on Google Earth Engine (https://earthengine.google.com/) and was used to derive the NDVI values for the entire Terrebonne Basin.

References

Abdi, H., & Williams, L. J. (2010). Tukey's honestly significant difference (HSD) test. *Encyclopedia of Research Design*, 3(1), 1–5.

Bertness, M. D. (1991). Zonation of Spartina patens and Spartina alterniflora in New England salt marsh. *Ecology*, 72(1), 138–148. https://doi.org/10.2307/1938909

Blum, M. D., & Roberts, H. H. (2009). Drowning of the Mississippi Delta due to insufficient sediment supply and global sea-level rise. *Nature Geoscience*, 2(7), 488–491. https://doi.org/10.1038/ngeo553

Booth, J. G., Miller, R. L., McKee, B. A., & Leathers, R. A. (2000). Wind-induced bottom sediment resuspension in a microtidal coastal environment. *Continental Shelf Research*, 20(7), 785–806. https://doi.org/10.1016/s0278-4343(00)00002-9

Cahoon, D. R., & Reed, D. J. (1995). Relationships among marsh surface topography, hydroperiod, and soil accretion in a deteriorating Louisiana salt marsh. *Journal of Coastal Research*, 357–369.

Chabreck, R. H., & Linscombe, R. G. (1982). Changes in vegetative types in Louisiana coastal marshes over a 10-year period. *Proceedings of the Louisiana Academy of Sciences*.

Chmura, G. L., Anisfeld, S. C., Cahoon, D. R., & Lynch, J. C. (2003). Global carbon sequestration in tidal, saline wetland soils. *Global Biogeochemical Cycles*, 17(4). https://doi.org/10.1029/2002gb001917

Christiansen, T., Wiberg, P. L., & Milligan, T. G. (2000). Flow and sediment transport on a tidal salt marsh surface. *Estuarine, Coastal and Shelf Science*, 50(3), 315–331. https://doi.org/10.1006/ecss.2000.0548

Chung, C. H. (2006). Forty years of ecological engineering with Spartina plantations in China. *Ecological Engineering*, 27(1), 49–57. https://doi.org/10.1016/j.ecoleng.2005.09.012

Clark, J. S., & Patterson, W. A. (1984). Pollen, Pb-210, and opaque spherules; an integrated approach to dating and sedimentation in the intertidal environment. *Journal of Sedimentary Research*, *54*(4), 1251–1265. https://doi.org/10.1306/212f85b2-2b24-11d7-8648000102c1865d

Connor, R., & Chmura, G. L. (2000). Dynamics of above-and belowground organic matter in a high latitude macrotidal saltmarsh. *Marine Ecology Progress Series*, *204*, 101–110. https://doi.org/10.3354/meps204101

Cortese, L., & Fagherazzi, S. (2022). Fetch and distance from the bay control accretion and erosion patterns in Terrebonne marshes (Louisiana, USA) [Dataset]. Earth Surface Processes Landforms, *47*, 1455–1465. https://doi.org/10.1002/esp.5327

Costa, Y., Martins, I., De Carvalho, G. C., & Barros, F. (2023). Trends of sea-level rise effects on estuaries and estimates of future saline intrusion. *Ocean & Coastal Management*, *236*, 106490. https://doi.org/10.1016/j.ocecoaman.2023.106490

Couvillion, B. R. (2021a). Coastal wetland area change in the Gulf of Mexico, 1985-2020 [Dataset]. U.S. Geological Survey Data Release. https://doi.org/10.5066/P9ZQI7ZW

Couvillion, B. R. (2021b). Coastal wetland area change in the Gulf of Mexico, 1985-2020. *U.S. Geological Survey Data Release*. https://doi.org/10.5066/P9ZQI7ZW

Couvillion, B. R., Beck, H., Schoolmaster, D., & Fischer, M. (2017). Land area change in coastal Louisiana (1932 to 2016). USGS scientific investigations map 3381. *U.S. Geological Survey*. Retrieved from https://pubs.usgs.gov/sim/3381/sim3381_pamphlet.pdf

Crichton, K. A., Anderson, K., Bennie, J. J., & Milton, E. J. (2015). Characterizing peatland carbon balance estimates using freely available Landsat ETM+ data. *Ecohydrology*, *8*(3), 493–503. https://doi.org/10.1002/eco.1519

Darby, F. A., & Turner, R. E. (2008). Below-and aboveground biomass of Spartina alterniflora: Response to nutrient addition in a Louisiana salt marsh. *Estuaries and Coasts*, *31*(2), 326–334. https://doi.org/10.1007/s12237-008-9037-8

DeLaune, R. D., Buresh, R. J., & Patrick, W. H., Jr. (1979). Relationship of soil properties to standing crop biomass of Spartina alterniflora in a Louisiana marsh. *Estuarine and Coastal Marine Science*, *8*(5), 477–487. https://doi.org/10.1016/0302-3524(79)90063-x

DeLaune, R. D., Jugsujinda, A., Peterson, G. W., & Patrick, W. H., Jr. (2003). Impact of Mississippi River freshwater reintroduction on enhancing marsh accretionary processes in a Louisiana estuary. *Estuarine, Coastal and Shelf Science*, *58*(3), 653–662. https://doi.org/10.1016/s0272-7714(03)00177-x

DeLaune, R. D., Kongchum, M., White, J. R., & Jugsujinda, A. (2013). Freshwater diversions as an ecosystem management tool for maintaining soil organic matter accretion in coastal marshes. *Catena*, *107*, 139–144. https://doi.org/10.1016/j.catena.2013.02.012

DeLaune, R. D., & Pezeshki, S. R. (1994). The influence of subsidence and saltwater intrusion on coastal marsh stability: Louisiana Gulf coast, USA. *Journal of Coastal Research*, 77–89.

DeLaune, R. D., Sasser, C. E., Evers-Hebert, E., White, J. R., & Roberts, H. H. (2016). Influence of the Wax Lake Delta sediment diversion on aboveground plant productivity and carbon storage in deltaic island and mainland coastal marshes. *Estuarine, Coastal and Shelf Science*, *177*, 83–89. https://doi.org/10.1016/j.ecss.2016.05.010

Dong, Z., Wang, Z., Liu, D., Song, K., Li, L., Jia, M., & Ding, Z. (2014). Mapping wetland areas using Landsat-derived NDVI and LSWI: A case study of west Songnen plain, Northeast China. *Journal of the Indian Society of Remote Sensing*, *42*(3), 569–576. https://doi.org/10.1007/s12524-013-0357-1

Donnelly, J. P., & Bertness, M. D. (2001). Rapid shoreward encroachment of salt marsh cordgrass in response to accelerated sea-level rise. *Proceedings of the National Academy of Sciences*, *98*(25), 14218–14223. https://doi.org/10.1073/pnas.251209298

Doughty, C. L., & Cavanaugh, K. C. (2019). Mapping coastal wetland biomass from high resolution unmanned aerial vehicle (UAV) imagery. *Remote Sensing*, *11*(5), 540. https://doi.org/10.3390/rs11050540

Engels, J. G., & Jensen, K. (2010). Role of biotic interactions and physical factors in determining the distribution of marsh species along an estuarine salinity gradient. *Oikos*, *119*(4), 679–685. https://doi.org/10.1111/j.1600-0706.2009.17940.x

Ewing, K. (1986). Plant growth and productivity along complex gradients in a Pacific northwest brackish intertidal marsh. *Estuaries*, *9*(1), 49–62. https://doi.org/10.2307/1352193

Gallant, A. L. (2015). The challenges of remote monitoring of wetlands. *Remote Sensing*, *7*(8), 10938–10950. https://doi.org/10.3390/rs70810938

Green, E. P., Mumby, P. J., Edwards, A. J., Clark, C. D., & Ellis, A. C. (1997). Estimating leaf area index of mangroves from satellite data. *Aquatic Botany*, *58*(1), 11–19. https://doi.org/10.1016/s0304-3770(97)00013-2

Greiner La Peyre, M. K., Grace, J. B., Hahn, E., & Mendelssohn, I. A. (2001). The importance of competition in regulating plant species abundance along a salinity gradient. *Ecology*, *82*(1), 62–69. https://doi.org/10.1890/0012-9658(2001)082[0062:tiocir]2.0.co;2

Gunter, G. (1956). Some relations of faunal distributions to salinity in estuarine waters. *Ecology*, *37*(3), 616–619. https://doi.org/10.2307/1930196

Guo, M., Li, J., Sheng, C., Xu, J., & Wu, L. (2017). A review of wetland remote sensing. *Sensors*, *17*(4), 777. https://doi.org/10.3390/s17040777

Howes, B. L., Howarth, R. W., Teal, J. M., & Valiela, I. (1981). Oxidation-reduction potentials in a salt marsh: Spatial patterns and interactions with primary production 1. *Limnology & Oceanography*, *26*(2), 350–360. https://doi.org/10.4319/lo.1981.26.2.0350

Howes, N. C., FitzGerald, D. M., Hughes, Z. J., Georgiou, I. Y., Kulp, M. A., Miner, M. D., et al. (2010). Hurricane-induced failure of low salinity wetlands. *Proceedings of the National Academy of Sciences*, *107*(32), 14014–14019. https://doi.org/10.1073/pnas.0914582107

Huete, A., Justice, C., & Van Leeuwen, W. (1999). MODIS vegetation index (MOD13). *Algorithm theoretical basis document*, *3*(213), 295–309.

Huete, A. R. (1988). A soil-adjusted vegetation index (SAVI). *Remote sensing of environment*, *25*(3), 295–309. https://doi.org/10.1016/0034-4257(88)90106-x

Ibñez, C., Curco, A., Day, J. W., & Prat, N. (2000). Structure and productivity of microtidal Mediterranean coastal marshes. *Concepts and Controversies in Tidal Marsh Ecology*, 107–136.

Janousek, C. N., Dugger, B. D., Drucker, B. M., & Thorne, K. M. (2020). Salinity and inundation effects on productivity of brackish tidal marsh plants in the San Francisco Bay-Delta Estuary. *Hydrobiologia*, *847*(20), 4311–4323. https://doi.org/10.1007/s10750-020-04419-3

Jensen, D. J., Cavanaugh, K. C., Thompson, D. R., Fagherazzi, S., Cortese, L., & Simard, M. (2022). Leveraging the historical Landsat catalog for a remote sensing model of wetland accretion in coastal Louisiana. *Journal of Geophysical Research: Biogeosciences*, *127*(6), e2022JG006794. https://doi.org/10.1029/2022jg006794

Jia, M., Wang, Z., Li, L., Song, K., Ren, C., Liu, B., & Mao, D. (2014). Mapping China's mangroves based on an object-oriented classification of Landsat imagery. *Wetlands*, *34*(2), 277–283. https://doi.org/10.1007/s13157-013-0449-2

Kearney, M. S., Stutzer, D., Turpie, K., & Stevenson, J. C. (2009). The effects of tidal inundation on the reflectance characteristics of coastal marsh vegetation. *Journal of Coastal Research West Palm Beach (Florida)*, *25*(6), 1177–1186. https://doi.org/10.2112/08-1080.1

Kelsall, M., Quirk, T., Wilson, C., & Snedden, G. A. (2023). Sources and chemical stability of soil organic carbon in natural and created coastal marshes of Louisiana. *Science of the Total Environment*, *867*, 161415. https://doi.org/10.1016/j.scitotenv.2023.161415

Kovacs, J. M., Flores-Verdugo, F., Wang, J., & Aspden, L. P. (2004). Estimating leaf area index of a degraded mangrove forest using high spatial resolution satellite data. *Aquatic Botany*, *80*(1), 13–22. https://doi.org/10.1016/j.aquabot.2004.06.001

Krauss, K. W., Duberstein, J. A., Doyle, T. W., Conner, W. H., Day, R. H., Inabinette, L. W., & Whitbeck, J. L. (2009). Site condition, structure, and growth of baldcypress along tidal/non-tidal salinity gradients. *Wetlands*, *29*(2), 505–519. https://doi.org/10.1672/08-77.1

Levine, J. M., Brewer, J. S., & Bertness, M. D. (1998). Nutrients, competition and plant zonation in a New England salt marsh. *Journal of Ecology*, *86*(2), 285–292. https://doi.org/10.1046/j.1365-2745.1998.00253.x

Li, L., Chen, Y., Xu, T., Liu, R., Shi, K., & Huang, C. (2015). Super-resolution mapping of wetland inundation from remote sensing imagery based on integration of back-propagation neural network and genetic algorithm. *Remote Sensing of Environment*, *164*, 142–154. https://doi.org/10.1016/j.rse.2015.04.009

Lopes, C. L., Mendes, R., Caçador, I., & Dias, J. M. (2020). Assessing salt marsh extent and condition changes with 35 years of Landsat imagery: Tagus Estuary case study. *Remote Sensing of Environment*, *247*, 111939. https://doi.org/10.1016/j.rse.2020.111939

Love, M. R., Caldwell, R. J., Carignan, K. S., Eakins, B. W., & Taylor, L. A. (2010). Digital elevation models of southern Louisiana: Procedures dataset. *Data Sources and Analysis*, *22*.

Lumbierres, M., Méndez, P. F., Bustamante, J., Soriguer, R., & Santamaría, L. (2017). Modeling biomass production in seasonal wetlands using MODIS NDVI land surface phenology. *Remote Sensing*, *9*(4), 392. https://doi.org/10.3390/rs9040392

Mendelssohn, I. A., & Kuhn, N. L. (2003). Sediment subsidy: Effects on soil–plant responses in a rapidly submerging coastal salt marsh. *Ecological Engineering*, *21*(2–3), 115–128. https://doi.org/10.1016/j.ecoleng.2003.09.006

Mo, Y., Kearney, M., & Momen, B. (2017). Drought-associated phenological changes of coastal marshes in Louisiana. *Ecosphere*, *8*(5), e01811. https://doi.org/10.1002/ecs2.1811

Mo, Y., Kearney, M. S., Riter, J. A., Zhao, F., & Tilley, D. R. (2018). Assessing biomass of diverse coastal marsh ecosystems using statistical and machine learning models. *International Journal of Applied Earth Observation and Geoinformation*, *68*, 189–201. https://doi.org/10.1016/j.jag.2017.12.003

Mo, Y., Momen, B., & Kearney, M. S. (2015). Quantifying moderate resolution remote sensing phenology of Louisiana coastal marshes. *Ecological Modelling*, *312*, 191–199. https://doi.org/10.1016/j.ecolmodel.2015.05.022

Morris, J. T., Sundareshwar, P. V., Nietch, C. T., Kjerfve, B., & Cahoon, D. R. (2002). Responses of coastal wetlands to rising sea level. *Ecology*, *83*(10), 2869–2877. https://doi.org/10.1890/0012-9658(2002)083[2869:rocwtr]2.0.co;2

Myneni, R. B., Keeling, C. D., Tucker, C. J., Asrar, G., & Nemani, R. R. (1997). Increased plant growth in the northern high latitudes from 1981 to 1991. *Nature*, *386*(6626), 698–702. https://doi.org/10.1038/386698a0

Neubauer, S. C. (2008). Contributions of mineral and organic components to tidal freshwater marsh accretion. *Estuarine, Coastal and Shelf Science*, *78*(1), 78–88. https://doi.org/10.1016/j.ecss.2007.11.011

Nyman, J. A., DeLaune, R. D., Roberts, H. H., & Patrick, W. H., Jr. (1993). Relationship between vegetation and soil formation in a rapidly submerging coastal marsh. *Marine Ecology Progress Series*, *96*, 269–279. https://doi.org/10.3354/meps096269

Nyman, J. A., Reid, C. S., Sasser, C. E., Linscombe, J., Hartley, S. B., Couvillion, B. R., & Villani, R. K. (2022). Vegetation types in coastal Louisiana in 2021 [dataset]. US Geological Survey Data Release. https://doi.org/10.5066/P9URYLMS

Nyman, J. A., Walters, R. J., Delaune, R. D., & Patrick, W. H., Jr. (2006). Marsh vertical accretion via vegetative growth. *Estuarine, Coastal and Shelf Science*, *69*(3–4), 370–380. https://doi.org/10.1016/j.ecss.2006.05.041

Nyman, J. A. A., DeLaune, R. D., & Patrick, W. H., Jr. (1990). Wetland soil formation in the rapidly subsiding Mississippi River deltaic plain: Mineral and organic matter relationships. *Estuarine, Coastal and Shelf Science*, *31*(1), 57–69. https://doi.org/10.1016/0272-7714(90)90028-p

Osland, M. J., Day, R. H., & Michot, T. C. (2020). Frequency of extreme freeze events controls the distribution and structure of black mangroves (Avicennia germinans) near their northern range limit in coastal Louisiana. *Diversity and Distributions*, *26*(10), 1366–1382. https://doi.org/10.1111/ddi.13119

Perez, B. C., Day, J. W., Jr., Rouse, L. J., Shaw, R. F., & Wang, M. (2000). Influence of Atchafalaya River discharge and winter frontal passage on suspended sediment concentration and flux in fourleague Bay, Louisiana. *Estuarine, Coastal and Shelf Science*, *50*(2), 271–290. https://doi.org/10.1006/ecss.1999.0564

Reed, D. J., Beall, A., Martinez, L., Minello, T. J., O'Connell, A. U., Rozas, L. P., et al. (2007). Modeling relationships between the abundance of fishery species, coastal wetland landscapes, and salinity in the Barataria basin, Louisiana. Final report to NOAA National marine Fisheries Service and the Louisiana coastal wetlands conservation and restoration task force. *The University of New Orleans*, 148p.

Ruan, L., Yan, M., Zhang, L., Fan, X., & Yang, H. (2022). Spatial-temporal NDVI pattern of global mangroves: A growing trend during 2000–2018. *Science of the Total Environment*, *844*, 157075. https://doi.org/10.1016/j.scitotenv.2022.157075

Ryo, M., & Rillig, M. C. (2017). Statistically reinforced machine learning for nonlinear patterns and variable interactions. *Ecosphere*, *8*(11), e01976. https://doi.org/10.1002/ecs2.1976

Sadler, P. M. (1981). Sediment accumulation rates and the completeness of stratigraphic sections. *The Journal of Geology*, *89*(5), 569–584. https://doi.org/10.1086/628623

Sanks, K. M., Shaw, J. B., & Naithani, K. (2020). Field-based estimate of the sediment deficit in coastal Louisiana. *Journal of Geophysical Research: Earth Surface*, *125*(8), e2019JF005389. https://doi.org/10.1029/2019JF005389

Sasser, C. E., Visser, J. M., Mouton, E., Linscombe, J., & Hartley, S. B. (2014). Vegetation types in coastal Louisiana in 2013. *U.S. Geological Survey Scientific Investigations Map 3290, 1 sheet, scale 1:550,000*. https://doi.org/10.3133/sim3290

Smart, R. M., & Barko, J. W. (1980). Nitrogen nutrition and salinity tolerance of Distichlis spicata and Spartina alterniflora. *Ecology*, *61*(3), 630–638. https://doi.org/10.2307/1937429

Snedden, G. A., Cretini, K., & Patton, B. (2015). Inundation and salinity impacts to above- and belowground productivity in Spartina patens and Spartina alterniflora in the Mississippi River deltaic plain: Implications for using river diversions as restoration tools. *Ecological Engineering*, *81*, 133–139. https://doi.org/10.1016/j.ecoleng.2015.04.035

Suir, G. M., & Sasser, C. E. (2019). Use of NDVI and landscape metrics to assess effects of riverine inputs on wetland productivity and stability. *Wetlands*, *39*(4), 815–830. https://doi.org/10.1007/s13157-019-01132-3

Sun, C., Fagherazzi, S., & Liu, Y. (2018). Classification mapping of salt marsh vegetation by flexible monthly NDVI time-series using Landsat imagery. *Estuarine, Coastal and Shelf Science*, *213*, 61–80. https://doi.org/10.1016/j.ecss.2018.08.007

Sun, C., Li, J., Cao, L., Liu, Y., Jin, S., & Zhao, B. (2020). Evaluation of vegetation index-based curve fitting models for accurate classification of salt marsh vegetation using sentinel-2 time-series. *Sensors*, *20*(19), 5551. https://doi.org/10.3390/s20195551

Sweet, W. V., Hamlington, B. D., Kopp, R. E., Weaver, C. P., Barnard, P. L., Bekaert, D., et al. (2022). Global and regional sea level rise Scenarios for the United States: Updated mean projections and extreme water level probabilities along U.S. Coastlines. NOAA Technical report NOS 01. National Oceanic and Atmospheric administration. *National Ocean Service*, 111. Retrieved from https://oceanservice.noaa.gov/hazards/sealevelrise/noaa-nos-techrpt01-global-regional-SLR-scenarios-US.pdf

Syvitski, J. P., Kettner, A. J., Overeem, I., Hutton, E. W., Hannon, M. T., Brakenridge, G. R., et al. (2009). Sinking deltas due to human activities. *Nature Geoscience*, *2*(10), 681–686. https://doi.org/10.1038/ngeo629

Tan, Q., Shao, Y., Yang, S., & Wei, Q. (2003). Wetland vegetation biomass estimation using Landsat-7 ETM+ data. In IGARSS 2003. 2003 IEEE international geoscience and remote sensing symposium. *Proceedings of IEEE Cat. No. 03CH37477*, *4*, 2629–2631.

Tilley, D. R., Ahmed, M., Son, J. H., & Badrinarayanan, H. (2007). Hyperspectral reflectance response of freshwater macrophytes to salinity in a brackish subtropical marsh. *Journal of Environmental Quality*, *36*(3), 780–789. https://doi.org/10.2134/jeq2005.0327

Törnqvist, T. E., Wallace, D. J., Storms, J. E., Wallinga, J., Van Dam, R. L., Blaauw, M., et al. (2008). Mississippi Delta subsidence primarily caused by compaction of Holocene strata. *Nature Geoscience*, *1*(3), 173–176. https://doi.org/10.1038/ngeo129

Turner, R. E., Swenson, E. M., & Milan, C. S. (2000). Organic and inorganic contributions to vertical accretion in salt marsh sediments. In *Concepts and controversies in tidal marsh ecology* (pp. 583–595). Springer.

Twilley, R. R., Bentley, S. J., Chen, Q., Edmonds, D. A., Hagen, S. C., Lam, N. S. N., et al. (2016). Co-evolution of wetland landscapes, flooding, and human settlement in the Mississippi River Delta Plain. *Sustainability Science*, *11*(4), 711–731. https://doi.org/10.1007/s11625-016-0374-4

Twilley, R. R., Day, J. W., Bevington, A. E., Castañeda-Moya, E., Christensen, A., Holm, G., et al. (2019). Ecogeomorphology of coastal deltaic floodplains and estuaries in an active delta: Insights from the Atchafalaya Coastal Basin. *Estuarine, Coastal and Shelf Science*, *227*, 106341. https://doi.org/10.1016/j.ecss.2019.106341

Valentine, K., Bruno, G., Elsey-Quirk, T., & Mariotti, G. (2021). Brackish marshes erode twice as fast as saline marshes in the Mississippi Delta region. *Earth Surface Processes and Landforms*, *46*(9), 1739–1749. https://doi.org/10.1002/esp.5108

Wang, F. C., Ransibrahmanakul, V., Tuen, K. L., Wang, M. L., & Zhang, F. (1995). Hydrodynamics of a tidal inlet in Fourleague bay/Atchafalaya bay, Louisiana. *Journal of coastal research*, 733–743.

Wang, Y., Colby, J. D., & Mulcahy, K. A. (2002). An efficient method for mapping flood extent in a coastal floodplain using Landsat TM and DEM data. *International Journal of Remote Sensing*, *23*(18), 3681–3696. https://doi.org/10.1080/01431160110114484

Weier, J., & Herring, D. (2000). Measuring vegetation (ndvi & evi). *NASA Earth Observatory*, *20*, 2.

Weston, N. B. (2014). Declining sediments and rising seas: An unfortunate convergence for tidal wetlands. *Estuaries and Coasts*, *37*(1), 1–23. https://doi.org/10.1007/s12237-013-9654-8

Wilson, B. J., Servais, S., Charles, S. P., Davis, S. E., Gaiser, E. E., Kominoski, J. S., et al. (2018). Declines in plant productivity drive carbon loss from brackish coastal wetland mesocosms exposed to saltwater intrusion. *Estuaries and Coasts*, *41*(8), 2147–2158. https://doi.org/10.1007/s12237-018-0438-z

Yuill, B., Lavoie, D., & Reed, D. J. (2009). Understanding subsidence processes in coastal Louisiana. *Journal of Coastal Research*, *10054*(10054), 23–36. https://doi.org/10.2112/si54-012.1

Zhang, M., Ustin, S. L., Rejmankova, E., & Sanderson, E. W. (1997). Monitoring Pacific coast salt marshes using remote sensing. *Ecological Applications*, *7*(3), 1039–1053. https://doi.org/10.1890/1051-0761(1997)007[1039:mpcsmu]2.0.co;2